Direction Sensing RFID Reader for Mobile Robot Navigation

Myungsik Kim, *Associate Member, IEEE*, and Nak Young Chong, *Member, IEEE*

***Abstract*—A self-contained direction sensing radio frequency identification (RFID) reader is developed employing a dual-directional antenna for automated target acquisition and docking of a mobile robot in indoor environments. The dual-directional antenna estimates the direction of arrival (DOA) of signals from a transponder by using the ratio of the received signal strengths between two adjacent antennas. This enables the robot to continuously monitor the changes in transponder directions and ensures reliable docking guidance to the target transponder. One of the technical challenges associated with this RFID direction finding is to sustain the accuracy of the estimated DOA that varies according to environmental conditions. It is often the case that the robot loses its way to the target in a cluttered environment. To cope with this problem, the direction correction algorithm is proposed to triangulate the location of the transponder with the most recent three DOA estimates. Theoretical simulation results verify the reliability of the proposed algorithm that quantifies the potential error in the DOA estimation. Using the algorithm, we validate mobile robot docking to an RFID transponder in an office environment occupied by obstacles.**

***Index Terms*—Direction finding, dual-directional antenna, mobile robot navigation, radio frequency identification (RFID).**

I. Introduction

ROBOTS are confronted with many difficulties when they are deployed into a real environment. Among the difficulties encountered in an indoor environment are how to accurately and efficiently identify and approach a specific object. Over the last few decades, a considerable number of studies have been performed on both identification and localization of objects [1]. One of the effective approaches is template-based visual recognition [2], [3], but this requires optical line-of-sight and is often significantly affected by the environmental conditions such as changes in illumination. Recent advances in sensor and networking technologies have provided new approaches aimed at structuring an easy-to-understand environment with networked embedded devices such as wireless sensors and radio frequency identification (RFID) transponders [4]–[6]. Such an environment helps the robot more easily retrieve complex information about the object, but does not usually support localization unless a GPS receiver is included in the system. The problem of location estimation thus remains a significant technical challenge in this approach.

Location estimating techniques can be classified as range-based and bearing-based. Range-based approaches trilaterate the transponder position using the estimated distance at reference points. Distances can be estimated from either received signal strength (RSS) measurements [7]–[9] or time-based methods using time-of-flight (TOF) [10] or time difference-of-arrival (TDOA) measurements [11], [12]. RSS-based schemes are easily implementable, but the accuracy is highly dependent on the environment and the distance. In contrast, it is possible to get fairly high accuracy using TDOA between RF and ultrasonic signals, but the ultrasonic signals are subject to multipath effects and the optical line of sight. To be more specific, a major difficulty with range-based schemes for mobile robot applications lies in the uncertainty of the robot's orientation. The robot needs to keep track of its heading to a target. On the other hand, bearing-based schemes use the direction-of-arrival (DOA) of a target. They have received more attention recently with arrays of multiple ultrasonic sensors [13], [14] and are considered to be better suited for mobile robot applications.

Therefore, our effort in this work is devoted to the development of a bearing-based ad hoc target acquisition and docking system using RFID technology for mobile robot applications. Our work is motivated by the fact that the directionality of the antenna can be incorporated into active RFID readers that typically use omnidirectional antennas. With such directional antennas installed, the robot becomes capable of easily identifying, locating, and tracking a target transponder. For this purpose, the direction sensing RFID reader equipped with the dual-directional antenna has been developed and demonstrated by the authors [15], [16]. Specifically, the DOA was achieved from the ratio of the RSS measurement between two adjacent antennas. This method was shown to be reliable and accurate for DOA estimation in an empty space. However, RF signals are easily distorted by the environmental effect that will significantly increase the error in the DOA estimation. This has been a major technical challenge for the engineers. In order to solve this problem, an effective direction correction algorithm is proposed using the geometric relations between the estimated directions with respect to the robot positions. The robot calculates the potential error included in the DOA estimation and adapts its direction of movement. The proposed algorithm is verified through extensive simulations and experiments.

This paper is organized as follows. In Section II, we briefly describe the proposed direction sensing RFID system and fundamentals of electromagnetic theory underlying the measurement of the DOA. Section III analyzes the multipath propaga-

Manuscript received February 01, 2007; revised July 20, 2007 and March 11, 2008. First published December 12, 2008; current version published December 30, 2008. This paper was recommended for publication by Associate Editor S. Sarma and Editor N. Viswanadham upon evaluation of the reviewers' comments. This research was conducted as a program for the "Fostering Talent in Emergent Research Fields" in Special Coordination Funds for Promoting Science and Technology in part by the Japan Ministry of Education, Culture, Sports, Science and Technology and in part by Korea MIC and IITA through IT leading R&D Support Program (2005-S-092-03, USN-Based Ubiquitous Robotic Space Technology Development).

The authors are with the School of Information Science, Japan Advanced Institute of Science and Technology, Ishikawa 923-1292, Japan (e-mail: reoreo93@gmail.com; nakyoung@jaist.ac.jp).

Digital Object Identifier 10.1109/TASE.2008.2006858

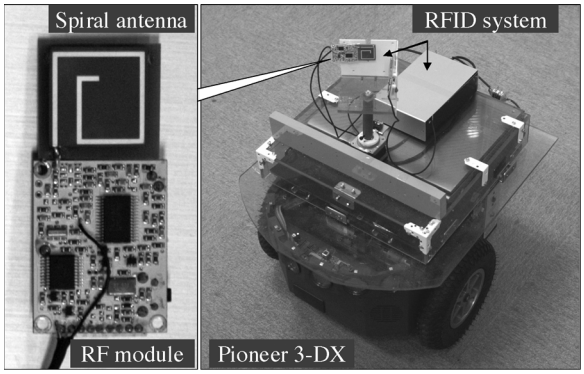

Fig. 1. Mobile robot equipped with direction sensing RFID reader.

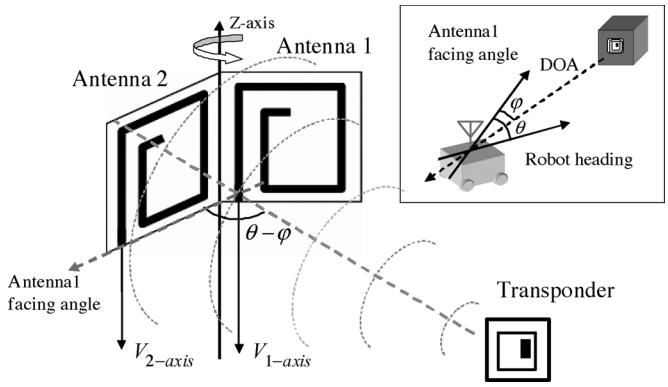

Fig. 2. Azimuth angle of the signal DOA in the dual-directional antenna.

tion to quantify the potential magnitude of errors in DOA estimation. The proposed direction finding algorithm is described in Section IV. Simulation and experimental results of mobile robot navigation based on the proposed algorithm are discussed in Section V. Finally, conclusions are drawn in Section VI.

II. Direction Sensing RFID Reader

Fig. 1 shows the target acquisition and docking system based on RFID. The system is composed of two parts: 1) an RFID reader interacting with active transponders and 2) a Pioneer 3-DX mobile robot onto which the reader is mounted. The RFID reader is developed using commercial active sensor nodes of Ymatic Limited [17] that operate on the 303.2 MHz frequency using a 3 V battery supply. A set of two nodes are used to develop the reader that reads the identification and strength of signals from other transponders using an AVR microcontroller through the RS-232C interface. The input signal within the range of 25 dBμVEMF to 80 dBμVEMF is converted linearly to a DC voltage ranging from 0.5 to 1.7 V. The reader can read multiple transponders at a time using the time-division multiple-access (TDMA) technique. The antenna is mounted on a rotating platform housed on top of the robot that is also controlled by the same AVR microcontroller. The size of the antenna is 20 mm $\times$ 20 mm that has a gain of -6.5 dBi with a wide beam width of 90°.

We now review the fundamental principles of DOA estimation from classical electromagnetic theory [18]. When an electromagnetic signal is transmitted to a directional antenna, as shown in Fig. 2, the magnetic flux Φ that passes through the antenna with the angle between the antenna surface plane and the signal wave plane can be represented as

$$\Phi = \frac{CSB}{r}\sin(\theta - \varphi) \tag{1}$$

where C accounts for environmental and operating conditions such as temperature, humidity, dust, and so on. S is the surface area of the antenna, B is the magnetic flux density of the wave passing through the antenna, r is the distance from the transponder, θ is the difference between the robot's heading and the facing angle of Antenna 1, and φ is the difference between the facing angle of Antenna 1 and the DOA of the signal, respectively. Here, we assume that the reader identifies transponders in the far-field region, i.e., r exceeds $\lambda/2\pi$ [19]–[21], thus the RSS is inversely proportional to r. The induced voltage at the antenna is proportional to the absolute value of the magnetic flux.

Note that the two spiral antennas in Fig. 2 have a phase difference of 90°, thus their induced voltage can be represented, respectively, as

$$V_1 \propto \left|\frac{CSB}{r}\sin(\theta - \varphi)\right| \tag{2a}$$

$$V_2 \propto \left|\frac{CSB}{r}\sin(\theta - \varphi + 90^\circ)\right|. \tag{2b}$$

Here, the angles are positive if they are measured in the counterclockwise direction around vertical axis of antenna plane. Now, we can define a dimensionless parameter as the ratio of magnitudes of induced voltages or signal strengths given by

$$\nu_{12} = V_1/V_2 = \left|\tan(\theta - \varphi)\right|. \tag{3}$$

Therefore, we can determine the DOA of signals φ from (3).

Fig. 3 shows an example of patterns and ratio of the RSS at the dual-directional antenna. The antenna scanned a transponder positioned 2 m away from -90° to 90° with respect to its facing direction in our experiment room. Since the room was not electromagnetically shielded, unknown environmental effects were included, thus we performed calibrations by adjusting the antenna direction, allowing two RSS curves to meet at zero degrees. Note that actual measured voltages may include an offset voltage, as shown in Fig. 3(a). Thus, according to the system's actual working and environmental conditions, the accuracy of the DOA estimation based on the ratio will be somewhat limited. This problem can be solved if we use the three points of interest which are shown as the minimum, maximum, and crossover (or inflection) points in Fig. 3(b). Despite the ratio pattern may vary due to the environmental and system conditions, those points always remain on the curve. Therefore, the DOA estimation can be achieved relying on the fact that, while the ratio increases, the transponder can be located in the direction of the crossover point within the range bounded by the minimum and maximum points.

III. Effects of RF Signal Multipath Propagation

It has been verified by our earlier experiments that the accuracy of the direction finding achieved with directional antennas remained within $\pm 4^\circ$ in an empty indoor environment [22].

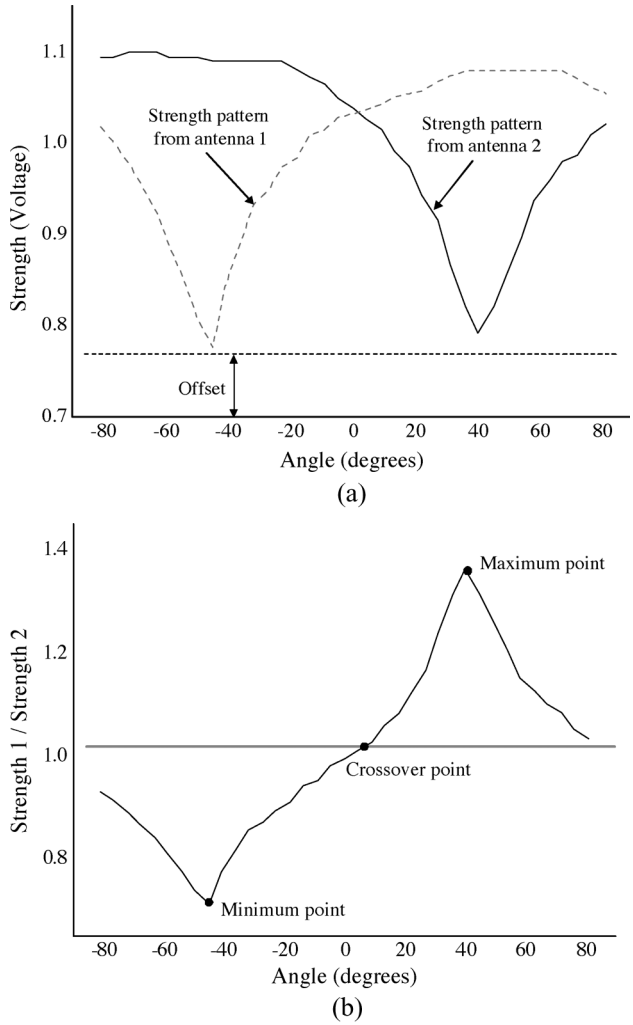

Fig. 3. An example of patterns and ratio of the RSS. (a) Pattern of signal strengths. (b) Ratio of signal strengths.

However, RF signals are easily distorted by obstacles, therefore the error increases in obstacle-cluttered environments. By the presence of the obstacles that reflect, refract, and scatter the propagated RF signal, the antenna receives a large number of RF signal with various amplitudes, phases, and directions, as shown in Fig. 4 [23], [24]. Thus, the total magnetic flux is the sum of the magnetic flux of the direct wave and that of the diffracted, nondirect waves represented by

$$\Phi_{\text{total}} = \Phi_{\text{direct}} + \sum_{i=1}^{n} \Phi^{i}_{\text{nondirect}} \tag{4}$$

where n is the total number of diffracted waves received at the antenna. Note that the magnetic flux density B can be written as

$$B = B_0 \sin(\kappa r - \omega t) \tag{5}$$

where B_0 is the amplitude of the magnetic flux density, κ is the propagation vector, r is the traveling distance of the wave, ω is the frequency of the transmitted wave, and t is the time, respectively.

By substituting (5) into (1), the magnetic flux can be expressed as

$$\Phi = \frac{CSRB_0 \sin(\kappa r - \omega t)}{r} \sin(\theta - \varphi) \tag{6}$$

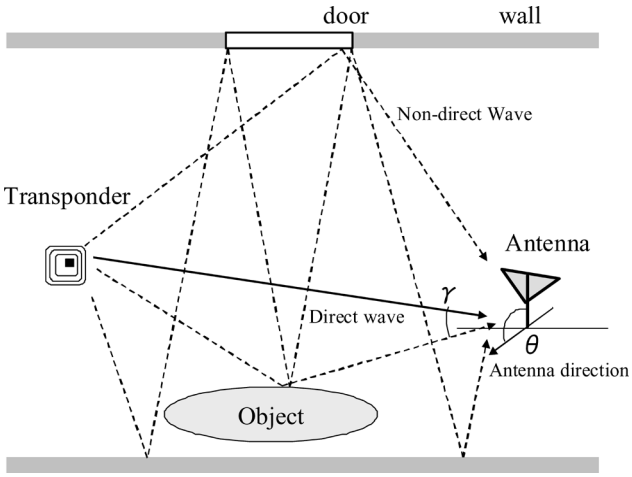

Fig. 4. An example of multipath propagation in indoor environments.

where R is the coefficient of the strength of the arrival signal (e.g., $R = 1$ when the wave is a nondiffracted, direct wave), and φ is the angle of incidence of each transmitted wave, respectively. For nondirect waves, r is the sum of the distances between the transponder and an obstacle, and between the obstacle and the antenna. In (6), the first term of the sine reflects the properties of the transmitted signal and the second term of the sine accounts for the changes in the RSS according to the antenna facing angles.

Assuming that direct and nondirect waves have differences in the angle of incidence γ_i, and the traveling distance Δr_i, respectively, (4) can be expanded as

$$\begin{aligned}\Phi_{\text{total}} = &\frac{CSB_0 \sin(\kappa r_0 - \omega t)\sin(\theta - \varphi_0)}{r_0} \\ &+ \frac{CSR_1B_0 \sin\left(\kappa r_0 - \omega t + \frac{2\pi\Delta r_1}{\lambda}\right)\sin(\theta - \varphi_0 + \gamma_1)}{r_0 + \Delta r_1} \\ &+ \ldots \end{aligned} \tag{7}$$

where λ is the wave length of the transmitted signal. In the equation, the phase difference between the direct and nondirect waves becomes $2\pi\Delta r_i/\lambda$, since there exists a difference in Δr_i.

If we denote the term $CSR_iB_0 \sin(\kappa r_0 - \omega t + (2\pi\Delta r_i/\lambda))/(r_0 + \Delta r_i)$ as a_i and $(\theta - \varphi_0)$ as χ, (7) can be rewritten as

$$\Phi_{\text{total}} = a_0 \sin(\chi) + a_1 \sin(\chi + \gamma_1) + \ldots. \tag{8}$$

Using the sum formula for sine, (8) can be transformed into

$$\begin{aligned}\Phi_{\text{total}} &= a_0 \sin(\chi) + a_1 \cos(\gamma_1)\sin(\chi) + a_1 \sin(\gamma_1)\cos(\chi) + \ldots \\ &= \left\{ a_0 + \sum_{i=1}^{n} a_i \cos(\gamma_i) \right\} \sin(\chi) \\ &\quad + \left\{ \sum_{i=1}^{n} a_i \sin(\gamma_i) \right\} \cos(\chi). \end{aligned} \tag{9}$$

After some mathematical manipulation, we can get the following equation:

$$\Phi_{\text{total}} = A \sin(\chi + \eta) \tag{10}$$

where

$$A = \left[\left(a_0 + \sum_{i=1}^{n} a_i \cos(\gamma_i) \right)^2 + \left(\sum_{i=1}^{n} a_i \sin(\gamma_i) \right)^2 \right]^{1/2} \tag{11a}$$

$$\eta = \tan^{-1} \left\{ \frac{\sum_{i=1}^{n} a_i \sin(\gamma_i)}{a_0 + \sum_{i=1}^{n} a_i \cos(\gamma_i)} \right\}. \tag{11b}$$

In (11), a_i varies according to Δr_i. The values Δr_i and γ_i reflect the relative locations between the transponder, the antenna, and the obstacles in the environment. Since the position of antenna will likely change linearly, Δr_i also changes linearly. Therefore, a_i periodically oscillates by the ratio between Δr_i and λ, while γ_i changes linearly. If there exist a number of obstacles, A and η are obtained by combining a variety of a_i and γ_i. Therefore, it is almost impossible to find the exact direction of the transponder in obstacle-populated environments. The worst case for the estimation error occurs when the denominator of η in (11b), $a_0 + \sum_{i=1}^{n} a_i \cos(\gamma_i)$ becomes zero. In this case, η increases or decreases to $\pm 90^\circ$. However, nondirect waves travel a longer distance than direct waves and their strength will be reduced by the obstruction. Thus, the magnitude of nondirect waves is much smaller than that of direct waves, and the denominator virtually does not become zero. Therefore, the estimation errors will be less than the maximum error of $\pm 90^\circ$.

Fig. 5 quantifies the possible magnitude of the DOA estimation error η calculated by (11) at each grid segment of 10 cm $\times$ 10 cm under various environmental conditions. In the figure, the black square shows the position of the transponder and the white circles are the position of obstacles. The intensity of gray level shows how much the propagated direction is distorted by the obstacles and is indicated as bar graph in degree on the right side of the figure. The strength of the signal reflected off the obstacle is assumed to be reduced by 80% (i.e., $R = 0.2$) for the left graph and 50% (i.e., $R = 0.5$) for the right graph, respectively.

Fig. 5(a) shows the error distribution of estimated directions when only one obstacle is located at $(-100, 0)$ cm. Note that errors increase when the obstacle has a larger value of R. In particular, a considerable amount of error exists in the area behind the obstacle. Fig. 5(b) shows the error distribution when the area is surrounded by seven obstacles located at $(-220, -220)$, $(-220, 0)$, $(-220, 220)$, $(0, -220)$, $(220, -220)$, $(220, 0)$, $(220, 220)$ cm, respectively. Some areas that have a large error near 90° appear irregularly with $R = 0.5$. The error pattern is similar to the interference fringe by the superposition of waves with various amplitude and phase differences. We can observe that the magnitude of the error irregularly oscillates in that area. Fig. 5(c) shows the case when three more obstacles are added at $(-100, -20)$, $(-100, 0)$, and $(-100, 20)$ cm, respectively. Similar to Case (a), the areas behind the obstacles display a large amount of errors. Fig. 5(d) shows the case when nine obstacles are randomly positioned in the area. We can find no regularity in the error distribution that changes according to the position of obstacles. When there exist many obstacles with a large R, the error may increase.

Fig. 6 is the statistical representation of Fig. 5. The whiskers range to the 90th percentile for tops and the 10th percentile for bottoms. The magnitude of the error varies according to the material properties and spatial distribution of the obstacles. Even though the propagation path of the transmitted signal is affected by the presence of obstacles, it is shown that the mean value of the error does not exceed 30°.

Fig. 7 shows the amount of errors that exist along the lines (i), (ii), and (iii) in Fig. 5(c) and (d). The dashed squares indicate the area that has a significantly large amount of errors. Note that the errors oscillate, but decrease in the area close to the transponder where the obstacles are not densely spaced.

When the robot moves along its estimated DOA, the distance between the robot and the transponder will increase or decrease, or remain unchanged according to the amount of error η. Table I shows the percentage of cases that the distance did not decrease among the results of Fig. 5. The total number of grid segments were counted that caused the robot to move away from the transponder. Here, the robot movement interval was set to the distance to the transponder divided by 5. It is shown that when R increases, the robot could move in the wrong direction. However, since the probability is quite small, the distance will decrease in most cases as the robot moves toward the transponder. Thus, if we devise a method that will enable the robot not to get stuck in the area where η can be very large, or it is ensured that η decreases as the robot moves, the robot can finally arrive at the target position. Therefore, in order to enable the robot not to lose its direction toward a transponder, we need to compensate for η.

IV. Algorithm for Accurate Direction Finding

As the robot estimates the direction it needs to go at a regular interval, the error will be propagated according to certain geometric relations between estimated directions and robot positions. In Fig. 8, let θ_i be the estimated direction with respect to the current heading of the robot, φ_i the exact direction of the target, and η_i the error between the estimated direction and the exact direction. Also let r_i be the distance between the transponder and the robot at the ith position that can be estimated from the RSS. When the robot moves in the direction of θ_i with an error of η_i, the distance to the transponder and the directions can be related by the following equation:

$$\frac{r_i}{\sin \eta_{i-1}} = \frac{r_{i-1}}{\sin \varphi_i}. \tag{12a}$$

It is known from the figure that $\varphi_i = \theta_i + \eta_i$, which can be substituted into (12a) to yield

$$\frac{r_i}{\sin \eta_{i-1}} = \frac{r_{i-1}}{\sin(\theta_i + \eta_i)}. \tag{12b}$$

Then, we can calculate the error at the $(i-1)$th position by summing the DOA estimation and its error at the ith position as

$$\eta_{i-1} = \sin^{-1} \left[\frac{r_i}{r_{i-1}} \sin(\theta_i + \eta_i) \right]. \tag{13a}$$

Similarly, the error at the $(i-2)$th position can be given by

$$\eta_{i-2} = \sin^{-1} \left[\frac{r_{i-1}}{r_{i-2}} \sin(\theta_{i-1} + \eta_{i-1}) \right]. \tag{13b}$$

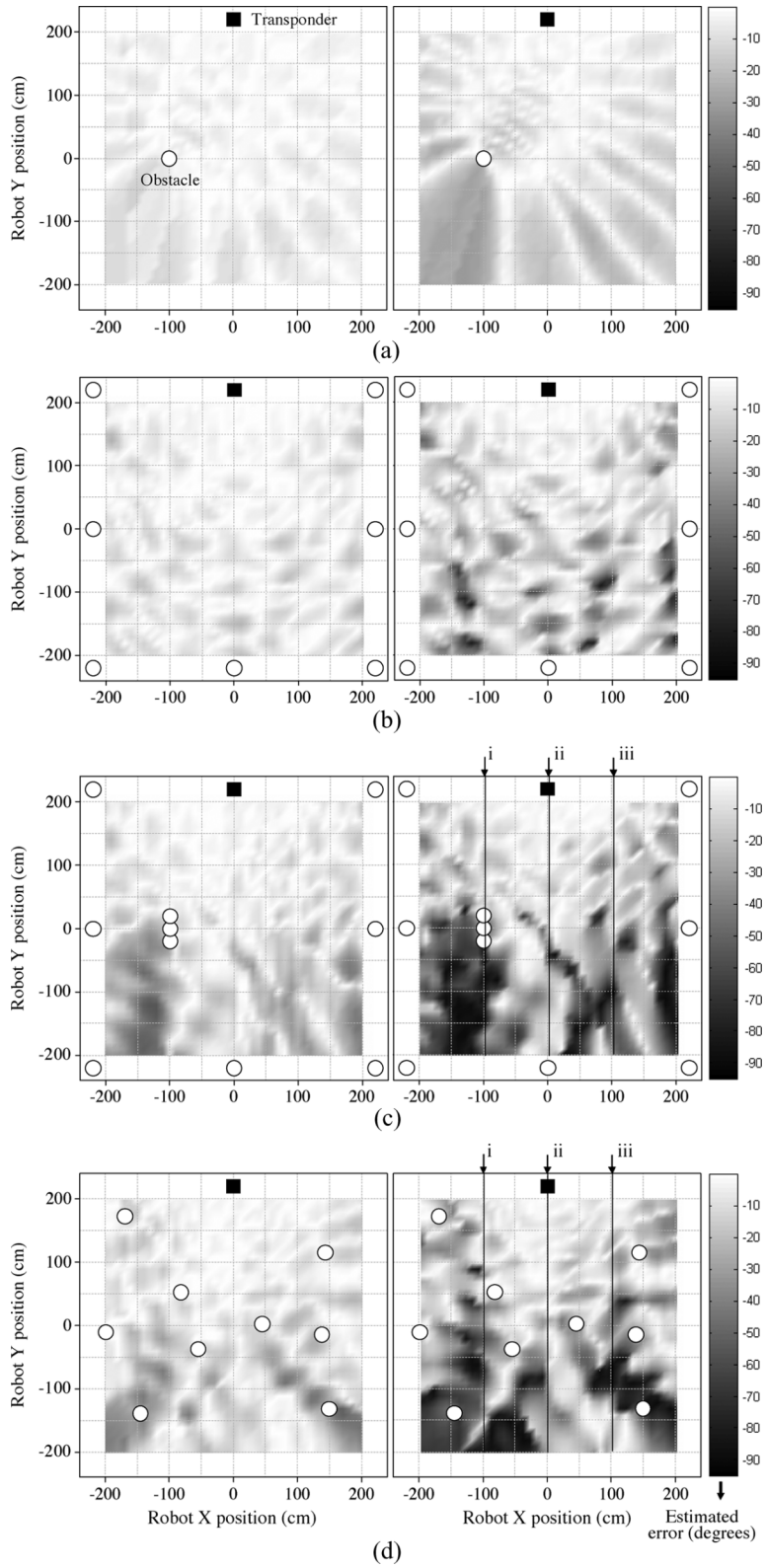

Fig. 5. Error in estimated direction by neighboring obstacles: (a) single obstacle at $(-100, 0)$; (b) surrounded by obstacles; (c) add obstacles around $(-100, 0)$ to the case of (b); and (d) randomly positioned obstacles.

Equations (13a) and (13b) give insight into how the error for the most recent measurement can be propagated back to adjust the error for the two previous estimations, provided that distance measurements are made at high accuracy. It is evident that distance measurement is critical to the accuracy of the above equations. It will be explained later in this section how to obtain at least semi-accurate estimation of distance.

Now, we explain how the estimated DOA can be corrected. It is almost impossible, in practice, to quantify the estimation error η_i. If we arbitrarily assume η_i at the ith robot position

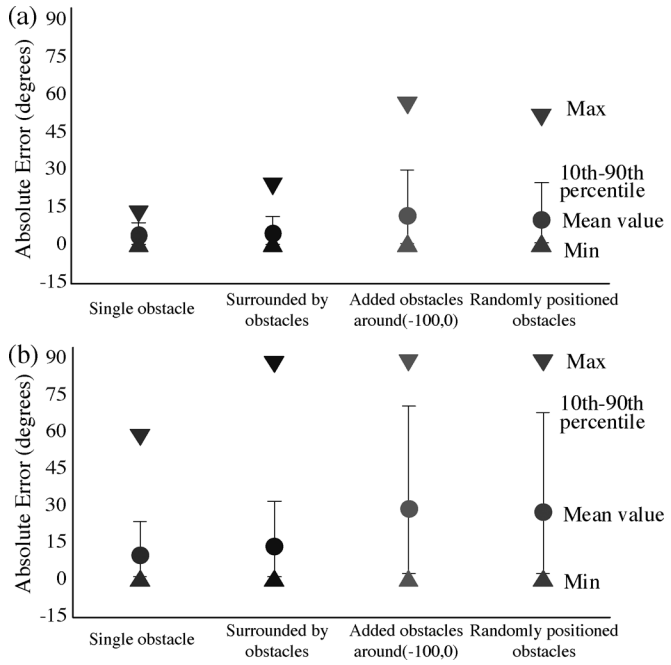

Fig. 6. Statistics of the direction sensing error in Fig. 5(a) reflecting (a) signal strength reduced by 80% ($R = 0.2$) and (b) reflecting signal strength reduced by 50% ($R = 0.5$).

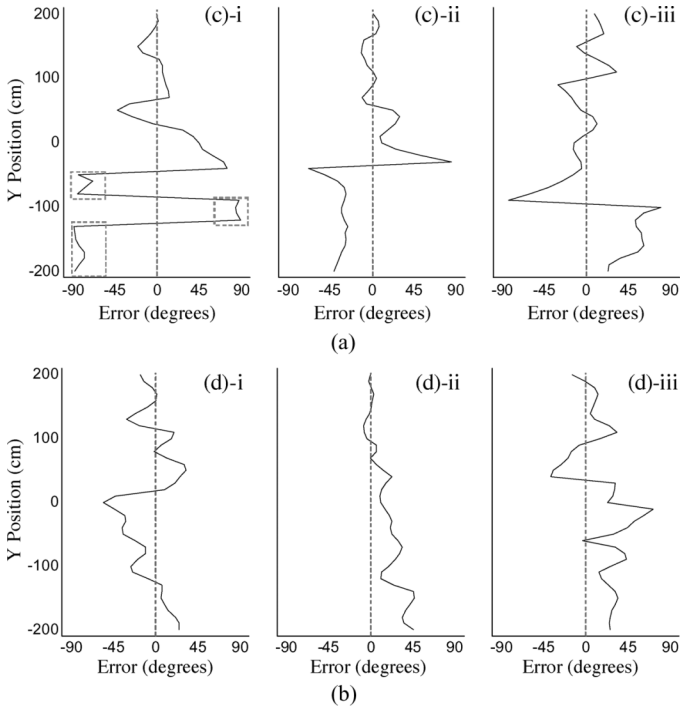

Fig. 7. Distortion errors of the propagated signal along the three lines in Fig. 5(c) and (d). (a) The case of Fig. 5(c). (b) The case of Fig. 5(d).

TABLE I
PERCENTAGE OF THE ESTIMATION THAT DOES NOT REDUCE THE DISTANCE TO THE TRANSPONDER

Environmental Conditions		Percentage (%)
R	Conditions of Fig. 5	
0.2	(a)	0
	(b)	0
	(c)	0
	(d)	0
0.5	(a)	0
	(b)	0.06
	(c)	2.85
	(d)	1.84

denoted as $\hat{\eta}_i$, the estimation error at the $(i-1)$th and $(i-2)$th robot positions, denoted as $\hat{\eta}_{i-1}$ and $\hat{\eta}_{i-2}$, respectively, will be determined according to (13a) and (13b). Thus, the estimation direction at each robot position will be continuously updated as $\hat{\eta}_i$ changes, as shown in Fig. 9. It should be noted that those three consecutive direction estimates may form a triangular area if we properly assume $\hat{\eta}_i$. Now, the most feasible direction of the target transponder can be determined by choosing $\hat{\eta}_i$ that makes as small a triangular area as possible, as shown in Fig. 9(iii). η_i at the ith robot position can, therefore, be quantified and the robot's heading can be controlled accordingly.

In order to implement the above scheme, as shown in Fig. 10, we define a Cartesian coordinate system whose origin is at the current position of the robot. Here, the y axis is assumed to be the direction obtained by the sum of the estimated direction θ_i and an arbitrary error $\hat{\eta}_i$. Then, the two previous positions of the robot can be written as

$$(x_{i-1}, y_{i-1}) = (-d_i \sin(\hat{\eta}_i + \theta_i), -d_i \cos(\hat{\eta}_i + \theta_i)) \quad (14a)$$

$$(x_{i-2}, y_{i-2}) = (x_{i-1} - d_{i-1} \sin(\hat{\eta}_i + \theta_i + \theta_{i+1}), \; y_{i-1} - d_i \cos(\hat{\eta}_i + \theta_i + \theta_{i+1})) \quad (14b)$$

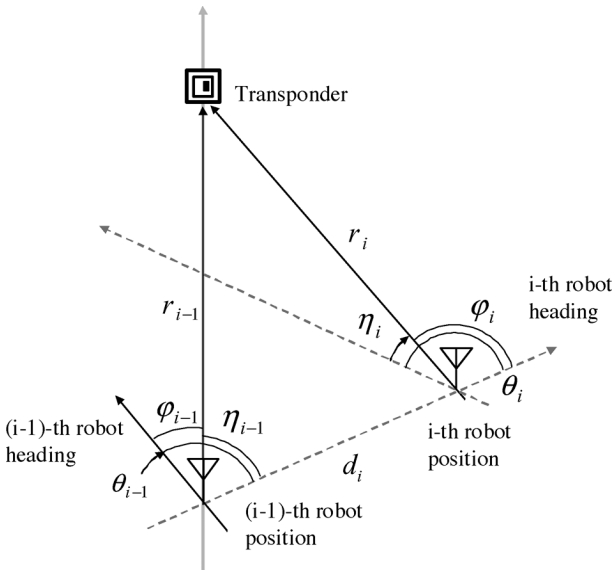

Fig. 8. Geometric relations between the positions of robot and transponder.

Now, the lines (i-1) and (i-2) starting at the two previous robot positions can be represented by

$$y = S_{i-1}(x - x_{i-1}) + y_{i-1} \quad (15a)$$

$$y = S_{i-2}(x - x_{i-2}) + y_{i-2} \quad (15b)$$

where

$$S_{i-1} = \cot(\hat{\eta}_i + \theta_i - \hat{\eta}_{i-1}) \quad (16a)$$

$$S_{i-2} = \cot(\hat{\eta}_i + \theta_i + \theta_{i-1} - \hat{\eta}_{i-2}). \quad (16b)$$

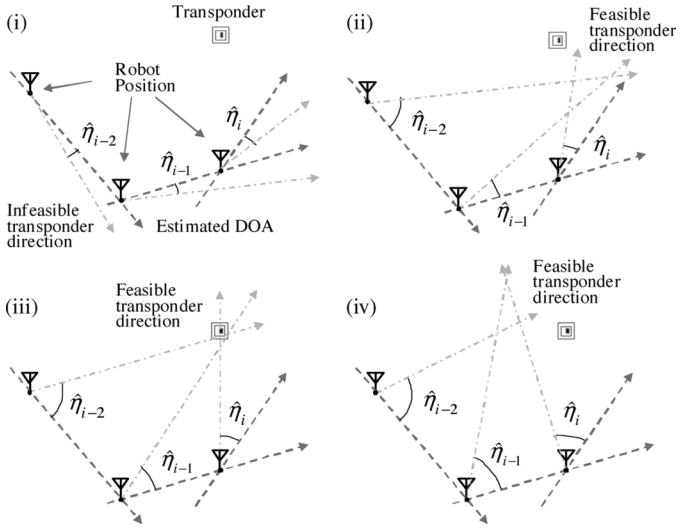

Fig. 9. Changes in the estimation error at robot positions according to $\hat{\eta}_i$: (i) lines do not form a triangular area; (ii)–(iv) lines form a triangular area; and (iii) choose $\hat{\eta}_i$ that minimizes the area.

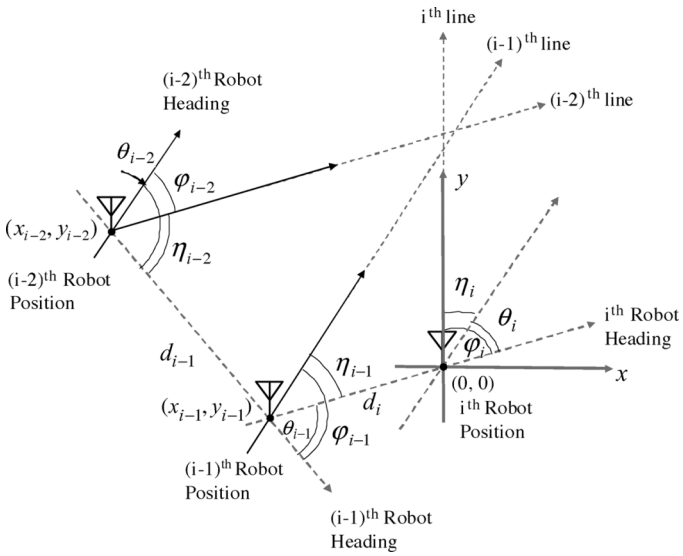

Fig. 10. Three directions of DOA estimation triangulates the transponder location.

Then, the lines (i-1) and (i-2) meet at a point whose x coordinate is represented as

$$x = \frac{S_{i-1}x_{i-1} - S_{i-2}x_{i-2} - y_{i-1} + y_{i-2}}{S_{i-1} - S_{i-2}}. \tag{17}$$

Since line (i) is the y-axis with which the two lines (i-1) and (i-2) form a triangle, x gives the size of possible potential location of the transponder.

If we go back to (13), the distance estimates r_i, r_{i-1}, and r_{i-2} are needed to find η_{i-1} and η_{i-2}. Note that the distance can be calculated from the RSS, but it is very difficult to obtain an accurate value of the RSS for accurate distance estimation. Since the accuracy of the DOA correction largely depends on the distance estimates, the expected measurement uncertainty will be resolved based on the following two factors.

1) The distance to the transponder mostly decreases as the robot moves following the estimation direction, as shown in Table I. This implies that r_i will not exceed r_{i-1}, which will allow the following inequality constraint to be satisfied:

$$\frac{r_i}{r_{i-1}} \leq 1. \tag{18a}$$

2) The difference of the distance of the transponder between two consecutive measurement points will not be greater than the moving interval of the robot. This implies that r_{i-1} will not exceed $r_i + d_i$, often referred to as the triangle inequality (see Fig. 8) given by

$$\frac{r_{i-1} - d_i}{r_{i-1}} \leq \frac{r_i}{r_{i-1}}. \tag{18b}$$

Now, the following inequality constraint can be imposed on r_{i-1} and r_i at each location when the robot moves a certain distance d_i:

$$\frac{r_{i-1} - d_i}{r_{i-1}} \leq \frac{r_i}{r_{i-1}} \leq 1. \tag{19}$$

Thus, the robot movement interval d_i can have significant effects on the range of reliability of distance estimates. For example, it has been reported that errors for RF signal strength estimates will not exceed around 20% in the general office environment [25]. Based on such information, r_i to the transponder 5 m away will be estimated within a range from 4 to 6 m. If d_i is a constant, say 50 cm, and the true r_{i-1} was 5.5 m at the previous measurement, r_{i-1} ranges from 4.4 to 6.6 m. Therefore, the maximum potential difference between r_i and r_{i-1} is 2.6 m that exceeds d_i, causing the apparent violation of (19). If such violation exists, we ignore r_{i-1} and obtain a new estimate $\hat{r}_{i-1}$ by adding one-half of d_i to r_i. This empirical approximation simplifies the task of estimating the uncertainty in distance measurements in (13).

In this work, η_i for the most recent measurement is assumed to be within the range of $n - 70°$ to $70°$. To triangulate the location of the transponder with three consecutive direction estimates, η_i is determined by the algorithm given next.

Algorithm 1: DOA Estimate Correction

Input : DOA estimates θ_{i-2}, θ_{i-1}, θ_i, distance estimates r_{i-2}, r_{i-1}, r_i, and robot moving interval d_{i-1}, d_i at three consecutive positions

Output: Error η_i included in θ_i

1 for $\hat{\eta}_i$ *changes from* $-70°$ *to* $70°$ *at* $5°$ *intervals* **do**

2 Re-estimate $\hat{r}_{i-2}$ and $\hat{r}_{i-1}$;

if $r_{i-1} - r_i > d_i$ **then**

$\hat{r}_{i-1} = r_i + d_i/2$;

else

$\hat{r}_{i-1} = r_{i-1}$;

if $r_{i-2} - \hat{r}_{i-1} > d_{i-1}$ **then**

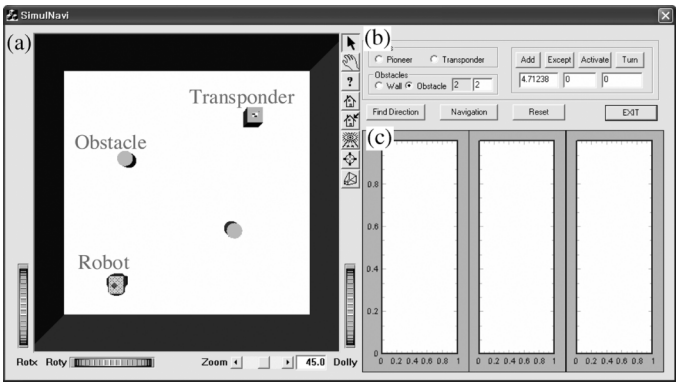

Fig. 11. Layout of the simulation program.

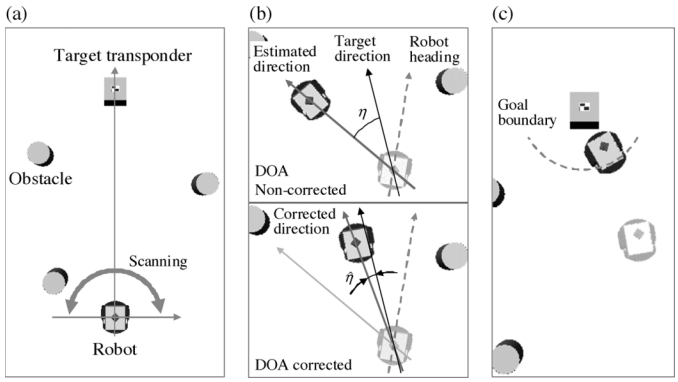

Fig. 12. Automated sequence of robot docking in the simulation. (a) The robot scans from -90° to 90° and estimates the target direction at its initial position (b) the robot moves following the estimated direction, or changes its direction employing the proposed algorithm (c) when the robot arrives within the range of 50 cm from the target transponder, it stops moving.

$\hat{r}_{i-2} = \hat{r}_{i-1} + d_{i-1}/2;$

else

$\hat{r}_{i-2} = r_{i-2};$

3 Calculate $\hat{\eta}_{i-1}$ and $\hat{\eta}_{i-2}$ using (13)

4 Calculate the potential location of transponder x using (17);

5 **if** $\hat{\eta}_i = -70^\circ$ **then**

The smallest x is determined as $x_{min} = x$;

$\eta_i = \hat{\eta}_i$;

else

if $x < x_{min}$ **then**

$x_{min} = x$

$\eta_i = \hat{\eta}_i$;

6 Return η_i, the error for the most recent measurement;

V. Simulation and Experimental Results of Robot Navigation

A. Simulation Results

To verify the validity of the proposed direction correction algorithm, we performed experiments on autonomous navigation using the simulator developed in-house, as shown in Fig. 11. Fig. 11(a) shows the simulation environment including a robot, a transponder, walls, and obstacles. The number of obstacles and the location of the robot can be modified by the control panel in Fig. 11(b). The path of the robot is displayed in Fig. 11(a) and the desired target direction, the estimated direction, and the estimation error are displayed in Fig. 11(c). Since it is almost impossible to include the whole scattering effect of signals in the obstacle-cluttered environment, we implemented the basic ray-tracing principle explained in the previous section.

The conditions used in the simulation are as follows.

- The size of the room is 5 m $\times$ 5 m.
- A transponder is considered as a point charge.
- The scattering of the signal by an obstacle is assumed to be occurring at the center of the obstacle, not the surface.
- All obstacles scatter signals with randomly determined rates.
- The robot is considered to receive signals associated with far-field regions.
- Intrinsic sensing error in the estimated direction is $\pm 4^\circ$ with the Gaussian distribution.

Under the above conditions, an automated docking sequence of the robot is performed according to the following steps, as shown in Fig. 12.

1) The robot scans the transmitted signal by rotating the antenna from -90° to 90° at its initial position and estimates the signal's DOA by finding the crossover points from the signal ratio curve [Fig. 12(a)].
2) The robot follows the estimated direction or changes its direction employing the proposed algorithm [Fig. 12(b)].
3) If the robot arrives within a reasonable range of the target, the robot stops moving [Fig. 12(c)]. We considered this case a success.
4) If the robot fails to arrive in the target area within a certain time limit, we consider that the robot failed to dock to the target.

Simulations were conducted under various test conditions, as shown in Fig. 13. In each condition, the left figure shows the case to which no direction correction algorithm is applied, and the right figure shows the case to which the direction correction algorithm is applied. Fig. 13(a) shows the results in an empty space. In this condition, there exists only an error of $\pm 4^\circ$ resulted from the intrinsic accuracy, thus the robot moves straight irrespective of whether the robot uses the proposed algorithm. Fig. 13(b) shows the condition that the area is surrounded by walls and obstacles similar to Fig. 5(c). Since the signal is distorted by the environmental effect, the robot navigates away from the obstacles. In contrast, it is shown that the proposed algorithm gives a straight path. In Fig. 13(c), where the robot navigates through randomly positioned obstacles, the robot can not reach the transponder position without using the proposed algorithm. As observed in the figure, the accuracy and robustness of DOA estimates is largely dependent on environmental

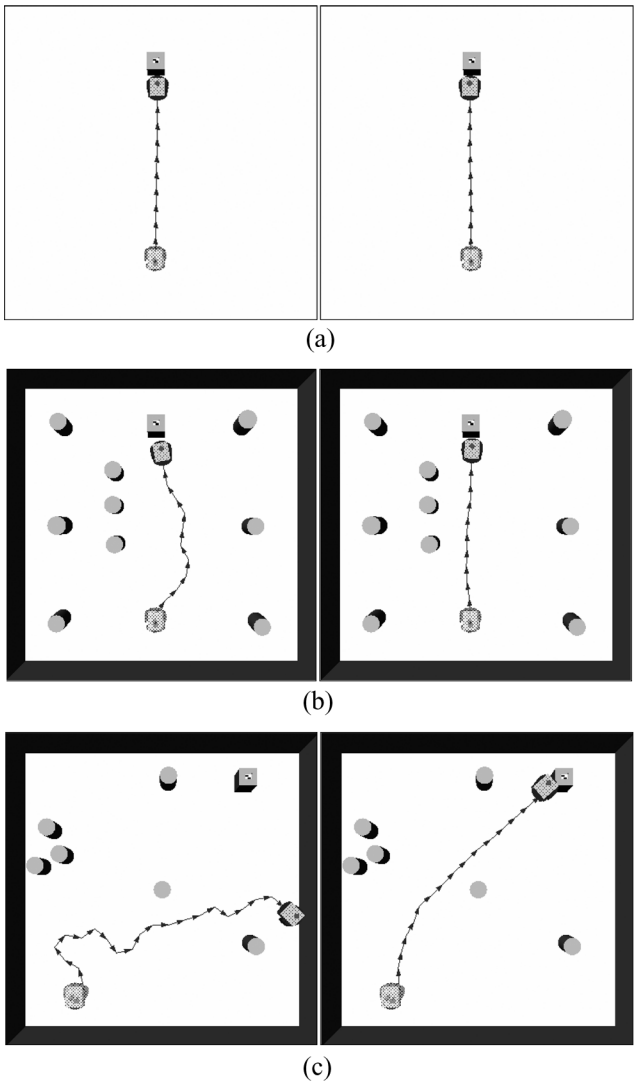

Fig. 13. Simulation results of DOA-guided docking under various conditions: (a) empty space; (b) space occupied by obstacles positioned at regular intervals and walls; and (c) space occupied by randomly positioned obstacles and walls.

conditions, but this does not mean that randomly positioned obstacles will cause a measurement error to be always too large.

Table II shows the results of docking to the target positioned 5 m away from the robot. Based on the DOA estimation, 50 trials were tested for each of six different environment conditions that differ in the number of obstacles. Therefore, a total of 300 trials were tested. Obstacles were randomly placed. When the signal was reflected off the obstacles, the strength was reduced by 50%. The same number of trials were tested for the same conditions employing the proposed algorithm. The success rate was higher in every case when the correction algorithm was employed.

The mean error in DOA estimation averaged over all successful trials and the 10th and 90th percentiles are compared in Fig. 14. If there were no substantial errors in DOA estimates, the error tended to increase by the correction algorithm, but remained within a reasonable range. It is evident that when the number of obstacles increased, larger errors occurred in DOA estimates.

TABLE II
CHANGES IN THE SUCCESS RATE WITHOUT/WITH THE CORRECTION ALGORITHM (SIMULATION)

No. of Obstacles	Without Algorithm			With Algorithm		
	Success	Fail	Rates (%)	Success	Fail	Rates (%)
0	50	0	100	50	0	100
1	50	0	100	50	0	100
3	50	0	100	49	1	98
5	40	10	80	46	4	92
7	28	22	56	42	8	84
9	19	31	38	37	13	74

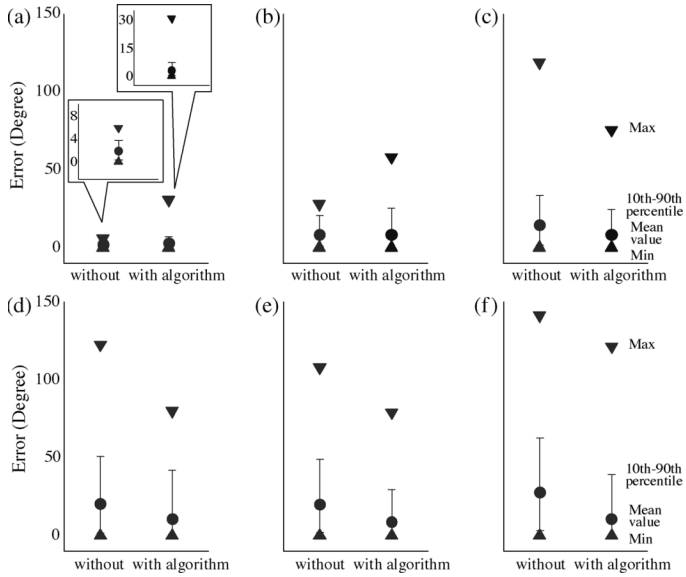

Fig. 14. Error in estimated direction according to the number of obstacles (simulation): (a) free space; (b) one obstacle; (c) three obstacles; (d) five obstacles; (e) seven obstacles; and (f) nine obstacles.

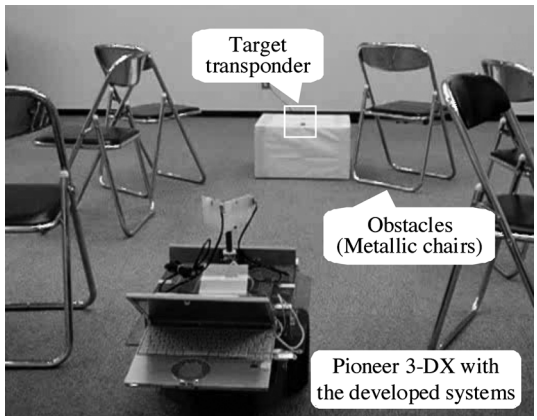

Fig. 15. Snapshot of the experiment.

B. Experimental Results

To verify the validity of the proposed algorithm in a real environment, we performed experiments with a Pioneer 3-DX mobile robot equipped with the developed direction sensing RFID system. Fig. 15 shows the snapshot of the test environment whose size is 6 m $\times$ 7 m. Experiments are performed near the center of the room. The target transponder is located at the position of (0, 3) m in a Cartesian coordinate system

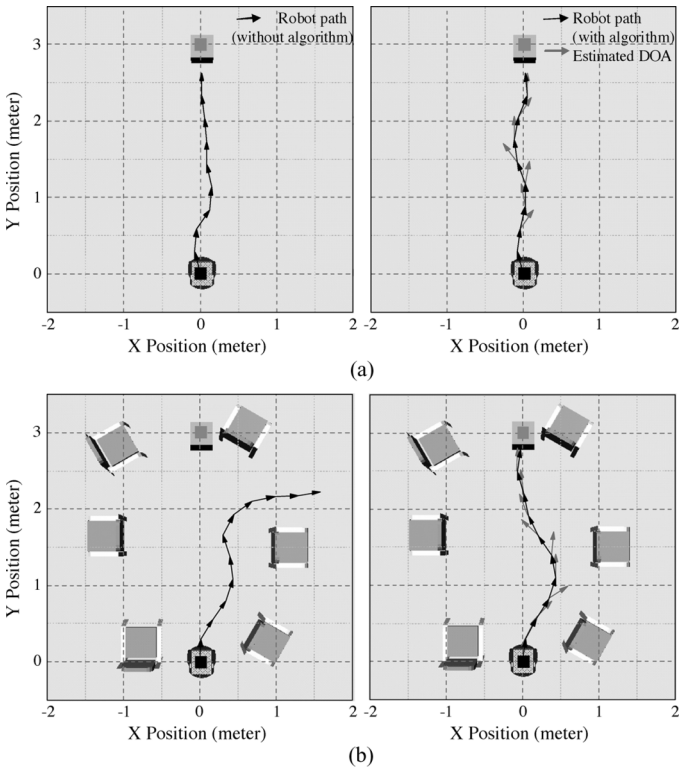

Fig. 16. Experimental results of DOA-guided docking under various conditions. (a) No obstacle positioned near from the path of the signal. (b) Obstacles positioned near the path of the signal.

TABLE III
CHANGES IN THE SUCCESS RATE WITHOUT/WITH THE PROPOSED ALGORITHM (EXPERIMENT)

No. of Obstacles	Without Algorithm			With Algorithm		
	Success	Fail	Rates (%)	Success	Fail	Rates (%)
0	10	0	100	10	0	100
6	7	3	70	9	1	90

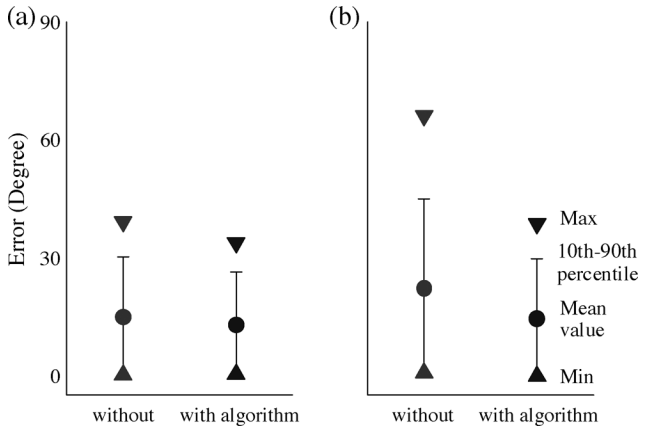

Fig. 17. Error in estimated direction without/with the correction algorithm (experiment): (a) empty space and (b) space with six metallic chairs.

whose origin is at the initial position of the robot. After the robot finds the direction to the transponder, the robot moves to the transponder guided by the RFID system. The robot stops approaching the transponder when the transponder is around the range of 50 cm from the robot. The distance is estimated from the signal strength and sonar sensors.

Ten trials were tested in our empty experiment room, and the same space with six metallic folding chairs, respectively. Fig. 16 shows the experimental results, where the black square indicates the initial position of the robot and the gray square is the target transponder position. The black arrows are the paths that the robot navigated. The left figures show the results of the robot docking guided by the noncorrected DOA estimation, and the right figures are the paths obtained by the proposed direction correction algorithm. To show the effect of the correction, the original DOA estimation in each step is also shown in the right figure by gray arrows. Fig. 16(a) shows the case that no obstacle is positioned near from the path of the direct signal. Thus, the robot can arrive at the transponder position in both cases. Note that the error in the DOA estimation varies according to the numbers, positions, and material properties of the obstacles. If the obstacles are located at the position that affects the transmission of the signals, the error increases. Fig. 16(b) shows the case where large DOA estimation errors occur when six chairs interfere with the transmission of the signal. The robot failed to dock to the transponder position by just following the original direction of DOA estimation. However, the robot using the proposed direction correction algorithm could arrive at the transponder position. Even though the gray arrow pointed to the wrong direction, the robot could find the right direction.

The success rates of target docking are summarized in Table III that compares the results of the proposed algorithm against those obtained without employing the algorithm. The changes in estimation error are also shown in both cases in Fig. 17. Since the environment was not electromagnetically shield, for instance, the walls might affect the DOA estimate. Thus, unknown errors occurred even when the space was empty, as shown in Fig. 17(a). Similar to the simulation results, errors increased when the environment was populated with obstacles. However, the algorithm keeps the direction accuracy within acceptable bounds, which indicates that the algorithm is practical and effective to reduce and correct the error included in DOA estimates.

In this work, we assume that a certain amount of estimation errors will always be present. Thus, if the estimates are very accurate (that do not necessarily need to be corrected) or the uncertainty associated with the robot's odometry and orientation increases, the accuracy of the proposed correction algorithm might deteriorate. Another difficulty may come from the relative magnitude of direct and nondirect waves. The received signal is the superposition of direct and nondirect waves with a different amplitude and phase, and the estimation error is the difference in the angle of incidence between the direct wave and the superposed waves. The amplitude (or intensity) of the direct wave is assumed to be larger than that of the nondirect waves. However, if the direct signal path between the transponder and the antenna is completely blocked, it may be possible to receive nondirect waves whose amplitude is much larger than that of the direct wave. This may cause a decrease in the accuracy of the algorithm.

VI. Conclusion

The dual-directional RFID antenna was proposed to enable autonomous navigation and docking for mobile robots in indoor environments. To cope with the uncertainties in the environment that was populated with obstacles, we proposed a robust direction finding algorithm that gave a fairly easy, yet good adjustment for DOA estimation. It only required the intervals of the robot movement, the DOA estimations, and the received signal strengths at the most recent three measurement points. The simulation and experimental results verified that the robot could arrive at the target position even though the RF signal was interfered with by obstacles. Our major contributions can be summarized as: 1) The proposed algorithm gives the most feasible direction to facilitate the finding of the transponder of interest when the robot suffers from an unknown amount of errors in DOA estimation. Therefore, 2) the proposed RFID reader improves the capability over the current state-of-the-art in RFID technology and can be applied to a variety of industrial applications. Our future effort includes the use of additional sensor data to be fused for enhancing the navigation capability of the robot in a more cluttered environment.

References

[1] J. Hightower and G. Borriello, "Location systems for ubiquitous computing," *IEEE Comput. Mag.*, vol. 34, no. 8, pp. 57–66, 2001.

[2] D. C. K. Yuen and B. A. MacDonald, "Vision-based localization algorithm based on landmark matching, triangulation, reconstruction, and comparison," *IEEE Trans. Robotics*, pp. 217–226, 2005.

[3] S. Se, D. G. Lowe, and J. J. Little, "Vision based global localization and mapping for mobile robots," *IEEE Trans. Robotics*, pp. 364–375, 2005.

[4] N. Y. Chong, H. Hongu, K. Ohba, S. Hirai, and K. Tanie, "A distributed knowledge network for real world robot applications," in *Proc. IEEE/RSJ Int. Conf. Intell. Robots Syst.*, 2004, pp. 187–192.

[5] L. E. Holmquist, H. W. Gellersen, G. Kortuem, S. Antifakos, F. Michahelles, B. Schiele, M. Beigl, and R. Maze, "Building intelligent environments with smart-its," *IEEE Comput. Graphics, Appl.*, vol. 24, no. 1, pp. 56–64, 2004.

[6] B. Brumitt, B. Meyers, J. Krumm, A. Kern, and S. Shafer, "Easy living: Technologies for intelligent environments," *Handheld and Ubiquitous Computing*, pp. 12–29, 2000.

[7] J. Hightower, G. Borriello, and R. Want, SpotON: An indoor 3D location sensing technology based on RF signal strength UW CSE Tech. Rep., Feb. 18, 2000.

[8] D. Niculescu and B. Nath, "Ad hoc positioning system (APS)," in *Proc. IEEE Global Telecomm. Conf.*, 2001, pp. 2926–2931.

[9] P. Bahl and V. N. Padmanabhan, "RADAR: An in-building RF-based user location and tracking system," in *Proc. IEEE INFOCOM*, 2000, vol. 2, pp. 775–784.

[10] S. Lanzisera, D. Lin, and K. Pister, "RF time of flight ranging for wireless sensor network localization," in *Proc. Workshop Intell. Solutions in Embedded Syst.*, 2006, pp. 1–12.

[11] A. Smith, H. Balakrishnan, M. Goraczko, and N. Priyantha, "Tracking moving devices with the cricket location system," in *Proc. 2nd Int. Conf. on Mobile Systems, Appl. Services*, 2004, pp. 190–202.

[12] L. M. Ni, Y. Liu, Y. C. Lau, and A. P. Patil, "LANDMARC: Indoor location sensing using active RFID," *ACM Wireless Networks*, vol. 10, no. 6, pp. 701–710, 2004.

[13] N. Priyantha, A. Chakaborty, and H. Balakrishnan, "The cricket location-support system," in *Proc. 6th ACM MOBICOM*, 2000, pp. 32–43.

[14] D. Niculescu and B. Nath, "Ad hoc positioning system (APS) using AOA," in *Proc. INFOCOM*, 2003, pp. 1374–1742.

[15] M. Kim and N. Y. Chong, "Enhancing RFID location sensing using a dual directional antenna," in *Proc. 6th Asian Control Conf.*, 2006, pp. 964–970.

[16] M. Kim, H. W. Kim, and N. Y. Chong, "Automated robot docking using direction sensing RFID," in *Proc. IEEE Int. Conf. Robot. Autom.*, 2007, pp. 4588–4593.

[17] [Online]. Available: http://www.ymatic.co.jp/

[18] D. Halliday, R. Resnick, and J. Walker, *Fundamentals of Physices*. New York: Wiley, 1997, pp. 579–594, 700–721, 753–758.

[19] K. Finkenzeller, *RFID Handbook: Fundamentals and Applications in Contactless Smart Cards and Identification*. New York: Wiley, 2003, pp. 112–114.

[20] W. L. Stutzman and G. A. Thiele, *Antenna Theory and Design*. New York: Wiley, 1999, pp. 28–31.

[21] C. A. Balantis, *Antenna Theory: Analysis and Design*. New York: Wiley, 1996, pp. 33–34.

[22] M. Kim and N. Y. Chong, Elsevier Science Ltd., "RFID-based mobile robot guidance to a stationary target," *Mechatronics*, vol. 17, no. 4–5, pp. 217–229, 2007.

[23] F. A. Alves, M. R. L. Albuquerque, S. G. Silva, and A. G. d'Assuncao, "Efficient ray-tracing method for indoor propagation prediction," in *Proc. SBMO/IEEE MTT-S Int. Conf. Microw. Optoelectronics*, 2005, pp. 435–438.

[24] L. Tsang and J. A. Kong, *Scattering of Electromagnetic Waves: Advanced Topics*. New York: Wiley, 2001.

[25] T. S. Rapaport, *Wireless Communications*. Englewood Cliffs, NJ: Prentice-Hall, 2002, pp. 157–166.

Myungsik Kim (S'04–A'07) received the B.S. and M.S. degrees in physics from Sogang University, Seoul, Korea, in 2001, and 2003, respectively, and the Ph.D. degree in robotics from the Japan Advanced Institute of Science and Technology (JAIST), Ishikawa, Japan, in 2007.

After receiving Ph.D. degree, he worked as Postdoctoral Researcher at JAIST until February 2008. While working for the M.S. degree, he developed the near-field scanning microscope using GHz range high-frequency signal. He researched the RFID-based robot docking system and the USN system for environment monitoring during his Ph.D. and postdoctoral researcher period. From March 2008, he was a Senior Researcher at the Ubiquitous Gwangyang and Global IT Institute, where he was engaged in the RFID-based identification system integration for iron and steel industry, and USN-based RTLS system development. Since September 2008, he has been a part-time Professor of Electronic Engineering at Sunchon National University, Sunchon, Korea.

Dr. Kim is a member of the Korea Association of RFID/USN.

Nak Young Chong (M'99) received the B.S., M.S., and Ph.D. degrees in mechanical engineering from Hanyang University, Seoul, Korea, in 1987, 1989, and 1994, respectively.

From 1994 to 1998, he was a Senior Researcher at Daewoo Heavy Industries, Ltd., where he was engaged in the development of welding robots and automation systems for shipbuilding fabrication and assembly processes, and the operation of underwater vehicles. During this period, he was a Visiting Researcher at the Biorobotics Division of Mechanical Engineering Laboratory, Tsukuba, Japa, from 1995–1996. After Daewoo Heavy Industries, Ltd., he spent one year at the Korea Institute of Science and Technology. From 1998 to 2003, he was on the research staff at the National Institute of Advanced Industrial Science and Technology, Tsukuba, Japan, doing networked robotics and ambient intelligence projects with the late Dr. K. Tanie. In 2003, he joined the faculty of the Japan Advanced Institute of Science and Technology as an Associate Professor of Information Science, where he currently directs the Robotics Laboratory.

Dr. Chong served as a Co-Chair of the IEEE RAS Technical Committee on Networked Robots from 2004 to 2006. He also served as a Co-Chair of the Fujitsu Scientific Systems Robotics Working Group from 2004 to 2006, and the Robot Information Processing Working Group from 2006–08, respectively. He visited the Laboratory for Intelligent Mechanical Systems at Northwestern University in 2001. He is currently on research leave from JAIST and Visiting Professor at the Center for Robotics and Intelligent Machines, Georgia Tech. He is the Korea Robotics Society Director of International Cooperation, and a member of RSJ and SICE.